entropy

MDPI

Article

Effects of Endwall Fillet and Bulb on the Temperature Uniformity of Pin-Fined Microchannel

Zhiliang Pan [1], Ping Li [1,*], Jinxing Li [1] and Yanping Li [2,*]

[1] Key Laboratory of Thermo-Fluid Science and Engineering, Ministry of Education, School of Energy and Power Engineering, Xi'an Jiaotong University, Xi'an 710049, China; pzl351304656@stu.xjtu.edu.cn (Z.P.); xing837439166@stu.xjtu.edu.cn (J.L.)

[2] School of Telecommunication and Information Engineering, Nanjing University of Posts and Telecommunications, Nanjing 210003, China

* Correspondence: pingli@xjtu.edu.cn (P.L.); liyp@njupt.edu.cn (Y.L.)

Received: 5 October 2017; Accepted: 14 November 2017; Published: 15 November 2017

Abstract: Endwall fillet and bulb structures are proposed in this research to improve the temperature uniformity of pin-fined microchannels. The periodical laminar flow and heat transfer performances are investigated under different Reynolds numbers and radius of fillet and bulb. The results show that at a low Reynolds number, both the fillet and the bulb structures strengthen the span-wise and the normal secondary flow in the channel, eliminate the high temperature area in the pin-fin, improve the heat transfer performance of the rear of the cylinder, and enhance the thermal uniformity of the pin-fin surface and the outside wall. Compared to traditional pin-fined microchannels, the flow resistance coefficient f of the pin-fined microchannels with fillet, as well as a bulb with a 2 μm or 5 μm radius, does not increase significantly, while, f of the pin-fined microchannels with a 10 μm or 15 μm bulb increases notably. Moreover, Nu has a maximum increase of 16.93% for those with fillet and 20.65% for those with bulb, and the synthetic thermal performance coefficient TP increases by 16.22% at most for those with fillet and 15.67% at most for those with bulb. At last, as the Reynolds number increases, heat transfer improvement of the fillet and bulb decreases.

Keywords: endwall fillet and bulb; microchannel heat sink; temperature uniformity; heat transfer enhancement; flow characteristic

1. Introduction

Energy and mass transfer process are involved in many industries, such as energy, transportation, aeronautics and astronautics, electronics, manufacturing, among which the heat exchanger plays a key role. With the development of science and technology and the increasing requirements of energy conservation and emission reduction, the heat exchange system has to promote the efficiency to meet the demand of higher heat intensity and thermal load. The high-efficient and energy-saving compact heat exchanger such as microchannel heat sink has gained more attraction in academic research and engineering applications [1].

The research on heat and mass enhancement based on flow control structures, such as pin-fin [2], groove [3], cavity [4], tip clearance [5], rib [6], dimple/protrusion [7], and bifurcation [8], is well conducted. Especially, the microchannel with pin-fins is widely used because of its high efficiency of heat transfer. Kosar et al. [9] studied the forced flow in the microchannel with staggered and in-line circular/diamond pin-fins array by experiment, and found that at low a Reynolds number, endwall effects and fin density influenced the flow resistance a lot, which was based on the proposition of modified correlations to predict the pressure drop in the microchannel. The Nusselt number, friction factor of water flow and thermal resistance in the microchannel with staggered pin-fin in a large range of heat fluxes were studied next [10]. Then, they found compact fins at a high Reynolds number

delayed the flow separation, thus depressed the endwall effect. Marques and Kelly [11] experimentally investigated the pressure loss and heat exchange of a micro heat exchanger with pin-fin array, and the results indicated that its heat exchange performances were all better than the corresponding parallel plate heat exchanger. Then, they proposed a cooling effectiveness prediction model for micro pin-fin heat exchanger in a gas turbine blade cooling application. Vanapalli et al. [12] analyzed the pressure penalty of a microchannel with compact pin-fin array. The results showed that among different cross section shapes, the sine-shaped pin-fin performed best when considering pressure penalty. The heat transfer of a microchannel with pin-fin in a large range of Reynolds numbers was experimentally studied by Wang et al. [13]. The results showed its heat transfer coefficient was twice that of the plate microchannel. What is more, the pin-fin with triangular cross section showed best heat transfer performance. The above studies show that arranging pin-fin in a microchannel is an effective heat transfer enhancement technique in high heat flux conditions.

As is shown in the above research results, the flow control structures enhance the whole heat exchange process in the microchannel, while on the walls in wake flow, corner vortex and separation bubbles, local high temperature regions still cannot be eliminated, indicating the deterioration of local heat transfer. Additionally, for the equipment under precision control, such as spacecraft and micro electronic devices, the deterioration of local heat transfer will increase the temperature gradient of the heat exchange surface, generate additional span-wise thermal resistance and influence the modulation response of the system a lot, which will threaten the safety of the equipment and economy and reliability of the system. Therefore, promoting the heat exchange surface thermal uniformity and eliminating local high temperature regions is significant for improving the efficiency and practicality of the microchannel heat sink with flow control structures.

Chyu [14] studied heat transfer performance of short pin-fined arrays with fillets, which was enveloped by a circular profile and arranged along the normal direction of channel, under $Re = 5000-30{,}000$. The results showed that the pin-fin endwall fillet deteriorated the heat transfer slightly at large *Re*. Furthermore, from the study of three-dimensional passage flow in compressors, the flow separation and channel secondary flow were found to be greatly influenced by the fillet. Cuyrlett [15] experimentally found that CDA (Controlled Diffusion Airfoil) blade with fillet increased the loss and secondary flow, while that for DCA (Double Circular Arc) blade with fillet showed the opposite trend. Hoeger et al. [16] numerically presented a "chamfer vortex", which was the opposite of the horseshoe vortex. The vortex could transfer the high energy fluid to the rear surface, suppress the separation of boundary layer in corner area, and enlarge the operating range of the multi-stage compressor. Hoeger et al. [17] analyzed the influence of the fillet and bulb on the endwall flow in the compressor cascade, and the results showed that the separation in the rear surface decreased and even disappeared under the influence of fillet structure. Kuegler et al. [18] numerically found that the fillet could decrease the corner separation and enlarge the range of throttling process in multi-stage compressor. Goodhand et al. [19] found that after removing the fillet, flow separation was enhanced considerably near the hub of stator blades in compressor and thus the loss was greater. Meyer et al. [20] found out in their experiment that the loss increased with the increment of the radius of fillet. All this research reveals that necessary designs on the fillet structures can beneficially influence the interaction between main flow and near wall flow and the heat exchange process by means of changing the separation flow structure of boundary layer near the corner region.

Therefore, to improve the uniformity of the temperature field, optimization of the microchannel with endwall filleted and bulbed pin-fin distributed in one side of the cylinder is carried out in this research. Laminar flow and heat transfer performances are studied with the Reynolds number ranging from 50 to 200 and the radius of fillet and bulb structures ranging from 0 to 15 μm, respectively. The flow pattern, temperature distribution and variations of performance parameters are comparatively analyzed.

2. Numerical Method and Validation

2.1. Geometrical Model and Boundary Conditions

Fully developed periodic velocity and temperature fields are obtained after several identical flow control devices arranged along stream-wise direction. For the flow and heat transfer process, most of the passage is in the periodic temperature field. Therefore, in our research minimal reduplicated unit is selected as computational domain to simplify the calculation process. The microchannel cross section is 200 μm (W) × 50 μm (H) and periodic length is 150 μm. In Figure 1, the coordinates x, y, z refer to the span-wise, stream-wise and normal-wise directions. A uniform constant heat flux of $q'' = 5 \times 10^5$ W·m^{-2} and no-slip boundary condition are set at four external surfaces and surfaces of the pin-fin device. Transitional periodic boundary condition is applied at the inlet and outlet surface. The main flow temperature is 300 K with the inlet Reynolds number ranging from 50 to 200.

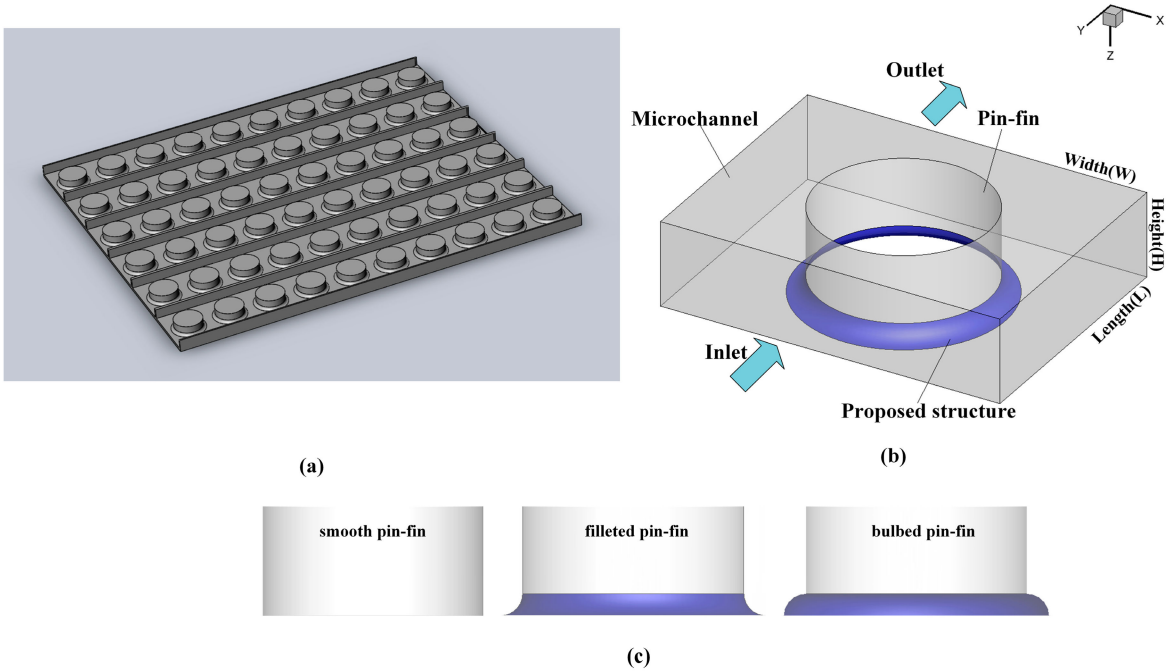

Figure 1. Microchannel heat sink and flow domain: (**a**) model of microchannel; (**b**) geometrical structures of flow domain; (**c**) geometry detail.

2.2. Governing Equation

Similar to our previous work [21], the incompressible inviscid steady water flow is assumed in this research. Therefore, the governing equations are as follows:

Continuity equation

$$\nabla \cdot \vec{u} = 0 \tag{1}$$

Momentum equation

$$\rho\left(\vec{u} \cdot \nabla\right)\vec{u} = -\nabla p + \mu\nabla^2\vec{u} \tag{2}$$

Energy equation

$$\rho C\left(\vec{u} \cdot \nabla T\right) = \lambda\nabla^2 T \tag{3}$$

The SIMPLE method is selected in coupling the pressure and velocity. The standard scheme is selected for pressure discretization and a second-order-up-wind scheme is selected for the momentum equation. The residuals of continuity, energy, and velocity components are selected to evaluate the convergence of the calculation process with the convergence criteria of 1×10^{-6}.

2.3. Parameter Definition

In this research, the work substance is water. Its thermo-physical properties are given in Table 1.

Table 1. Thermo-physical properties of water.

Substances	$k\ (\mathbf{W \cdot m^{-1} \cdot K^{-1}})$	$\mathbf{C}_p\ \left(\mathbf{J \cdot kg^{-1} \cdot K^{-1}}\right)$	$\rho\ (kg \cdot m^{-3})$	$\mu\ (Pa \cdot s)$
water	0.6	4180	998.2	9.93×10^{-4}

The Reynolds number is defined by

$$Re = \frac{\rho U_{m,in} D_h}{\mu} \tag{4}$$

where $U_{m,in}$ is the average velocity of the inlet surface, D_h is the hydraulic diameter and can be calculated by

$$D_h = \frac{2WH}{W+H} \tag{5}$$

The Nusselt number is defined by

$$Nu = \frac{hD_h}{\lambda} \tag{6}$$

where λ is the thermal conductivity of fluid. Heat transfer coefficient h is described as

$$h = \frac{q''}{\Delta T} \tag{7}$$

where q'' represents the heat flux. ΔT refers to the difference between average temperature of walls $T_{w,ave}$ and average fluid temperature $T_{f,ave}$

$$\Delta T = T_{w,ave} - T_{f,ave} \tag{8}$$

The Fanning friction is calculated by

$$f = -\frac{(\Delta P/L)D_h}{2\rho U_{ave,in}^2} \tag{9}$$

where ΔP is the pressure drop, ρ is the density of fluid, L represents the stream-wise microchannel length.

In the forced conductive flow with heat transfer, the entropy generation contains two parts, one caused by the heat transfer irreversibility, and the other due to the fluid frictional irreversibility [22]. The entropy generation of flow can be calculated by the following equations [23]

$$S' = \frac{\lambda}{T^2}\left(|\nabla T|\right)^2 + \frac{\mu}{T}\left(\frac{\partial U_i}{\partial x_j} + \frac{\partial U_j}{\partial x_i}\right)\frac{\partial U_i}{\partial x_j} = S'_T + S'_F \tag{10}$$

$$S'_T = \frac{\lambda}{T^2}\left(|\nabla T|\right)^2 \tag{11}$$

$$S'_F = \frac{\mu}{T}\left(\frac{\partial U_i}{\partial x_j} + \frac{\partial U_j}{\partial x_i}\right)\frac{\partial U_i}{\partial x_j} \tag{12}$$

where T refers to the temperature of water.

As for the internal microchannel flow, the entropy generating rate per unit length is calculated by [23]

$$S' = \frac{1}{\pi Nu}\frac{q'^2}{\lambda T^2} + \frac{m^3 f}{\pi^2 \rho^2 T r^5} \tag{13}$$

q' and r are defined by

$$q' = 2\pi r_0 q'', r = \frac{D_h}{2} \tag{14}$$

Therefore, Equation (13) can be given as

$$S' = \frac{q''^2 \pi D^2}{\lambda T^2 Nu} + \frac{32m^3}{\pi^2 \rho^2 T} \frac{f}{D^5} = S'_T + S'_F \tag{15}$$

2.4. Model Validation

In order to increase the accuracy and validity of our model, an all-hexahedral mesh is generated and improved. To balance the accuracy and computational resource, we performed a grid independence validation to determine the optimal grid nodes for the following numerical analysis. Four different meshes are generated and studied with the grid node of 400,824, 1,329,900, 2,475,960 and 3,926,120 (under the circumstance of $q'' = 5 \times 10^5$ W·m^{-2}, T_{in} = 300 K, Re = 100, r = 5 μm). The results are shown in Table 2. The relative discrepancies of Nu and f are 0.07% and −0.16% respectively when the mesh changes from Mesh 2 to Mesh 3. Hence, the optimal mesh is Mesh 2. Meshes with other geometrical structures choose similar mesh size. Using the model above, the numerical simulation in the corresponding smooth microchannel with a height of 200 μm, a width of 50 μm and a length of 150 μm has been conducted, and Table 3 shows that the differences of fRe and Nu compared with the results in reference [24] are no more than 1%, which ensures the accuracy and reliability of the model.

Table 2. Grid independence validation.

Mesh	Nodes	*Nu*	Difference %	*f*	Difference %
1	400,824	5.180	−0.53	0.557	0.04
2	1,329,900	5.152	−0.12	0.558	−0.16
3	2,475,960	5.146	−0.07	0.557	−0.16
4	3,926,120	5.143	-	0.556	-

Table 3. Simulation model validation.

Re	fRe			Nu		
	Referenced Result	Proposed Model	Difference %	Referenced Result	Proposed Model	Difference %
50	18.233	18.136	−0.53	2.94	2.930	−0.35
100	18.233	18.300	−0.37	2.94	2.914	0.87
200	18.233	18.344	0.61	2.94	2.954	0.46

3. Results and Analysis

3.1. Flow Structure and Temperature Distribution

The temperature distribution with limiting streamlines on the wall, and temperature distribution with streamlines on the span-wise middle section are used to analyze the detailed flow structures and heat transfer performance in this study.

Figure 2 shows the temperature distribution with limiting streamlines on the pin-fin with fillet and bulb, and surrounding walls when the Reynolds number is 50, and the radius of fillet and bulb ranges from 0 μm to 15 μm. When Re = 50, as the radius increases, the high temperature region A in the rear side of smooth pin-fin decreases gradually, and the temperature also goes down. When r = 15 μm, the temperature in region A is slightly above the average temperature of the rear side, and the high temperature area disappears. It is obvious that the fillet and bulb weaken the symmetry of the flow field along the normal-wise direction, and the fluid from the rear side has the trend to flow upward, so the

flow structure in region A has been improved. As the radius increases, the fillet and bulb influence the flow field even more, thus the high temperature region A decreases gradually. The temperature change trend of region B in rear side with proposed flow structures is the same with that of region A, but because of the direct effect of the fillet and bulb, the effects in region B are more obvious, and the high temperature area already disappears when r = 10 μm. The flow in this area cools the wall surface more intensely, which significantly improves the heat and mass transfer in region B and thus greatly improves the local temperature uniformity. For region C in the side surface of the pin-fin, the temperature decreases with the increase of the radius, which means both the fillet and bulb strengthen the heat transfer process near the surface of the pin-fin at a low Reynolds number. Especially, the bulb makes the low temperature area move from the side surface of the pin-fin to the bulb when the radius is larger than 10 μm. For the fillet and bulb, the changes of temperature distribution in the bottom wall region D which is in contact with the fillet and bulb differ from each other as the radius increases. For the pin-fin with fillet, the temperature gradient decreases gradually, and the low temperature region gradually increases as the radius increases. When r = 15 μm, the low temperature area occupies almost the whole mainstream area, and the overall thermal uniformity of the bottom wall is improved. For the pin-fin with bulb, the increase of the radius leads to the temperature decreases at all bottom walls, but it also results in the increase of temperature gradient gradually. For the leading edge of the pin-fin region E, its temperature decreases and approaches to the low temperature zone on both sides of the pin-fin with the increase of the radius. The triangle-shape high temperature area in this region decreases with the radius increasing, and it is more pronounced on the bottom side.

From the above analysis, the proposed structures significantly lower the temperature of the rear side surface, leading edge and side surface of the pin-fin and shrink the high temperature area, and its effect increases as the radius increases. The proposed flow structures improve the temperature uniformity of the microchannel, which can be useful for the laminar heat transfer enhancement researches employing triangular, square and circular pin-fins [25–28].

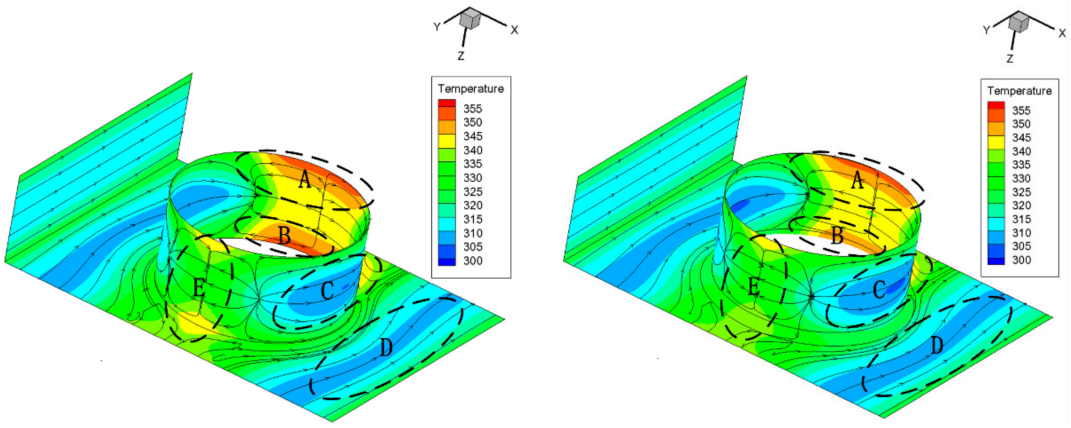

Figure 2. *Cont.*

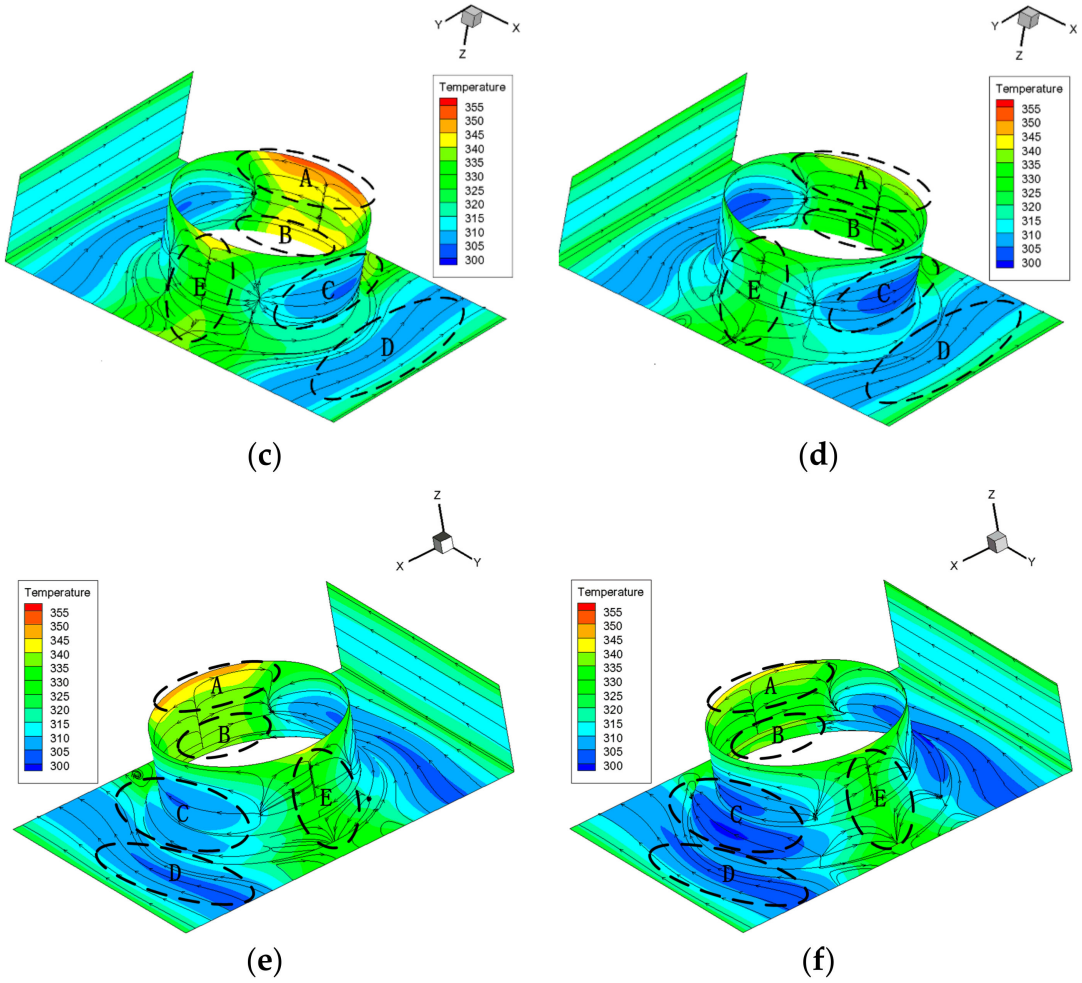

Figure 2. The distribution of temperature (unit: K) and limiting streamlines on the wall (*Re* = 50): (**a**) *r* = 0 μm; (**b**) *r* = 5 μm; (**c**) *r* = 10 μm; (**d**) *r* = 15 μm; (**e**) *ro* = 10 μm; (**f**) *ro* = 15 μm.

As shown in Figure 3, when *Re* = 200, compared to Figure 2, the highest temperature region of pin-fin with both fillet and bulb has changed from the rear of the cylinder to the vortex region near the corner when *Re* changes from 50 to 200. The high temperature region N is shrinking and cooling with the increment of the radius, which indicates that the local flow and heat transfer is refined. This is because the fillet and bulb enhance the mass transfer and admixture between the main flow and near-surface flow, decrease the average temperature of the bottom surface and the temperature gradient and intensify the heat and mass transfer near the vortex region. The same trend appears in the region near the side surface, which is highly expected and reasonable because with the increase of the velocity of the fluid, the fluid will wash the wall surface more violently which thus improves the heat transfer there. However, region M is expanding and heating with the increment of the radius, which indicates that flow and heat transfer deteriorates. The same trend appears on the top surface near the rear of the cylinder. This is because, at a high Reynolds number, the vortex in the corner and in wake of the rear of the cylinder is stronger, which suppresses the influence of the fillet and bulb on the flow on the top surface and region M, constrains the effect of the proposed structure to the lower half in the microchannel, limits it to develop in the span-wise direction and makes the low temperature flow away from the top surface. Besides, in the side surface of the cylinder, the temperature increases as the radius increases. With the increase of the radius, the geometrical structure in z direction becomes more asymmetrical, which induces an asymmetrical flow field, with more violent flow washing the bottom. Thus, the asymmetrical flow field causes differences of heat transfer between region M and region

N. The asymmetrical field makes it more difficult to evaluate the whole heat transfer performance. Therefore, more analysis is needed to find out whether the whole heat transfer performance is improved considering that different regions have different trends. Different structures also make a difference. For the result of pin-fin with bulb, compared to the result of pin-fin with fillet structure, a relatively higher temperature area appears in region L. Additionally, in region K it is interesting to note that the back flow in the rear in those with bulb shifts ahead compared to that with fillet. This phenomenon can explain the flow pattern differences in region L between two structures: The back flow with bulb causes more flow separation in the rear of the cylinder surface. This leads to the deterioration of heat transfer and thus the expansion of region L in the cases with bulb. Besides, the distribution of temperature field when *Re* is 200 is similar to that of a *Re* of 50 around the bottom area except that those with bulb have an undesirable greater temperature gradient.

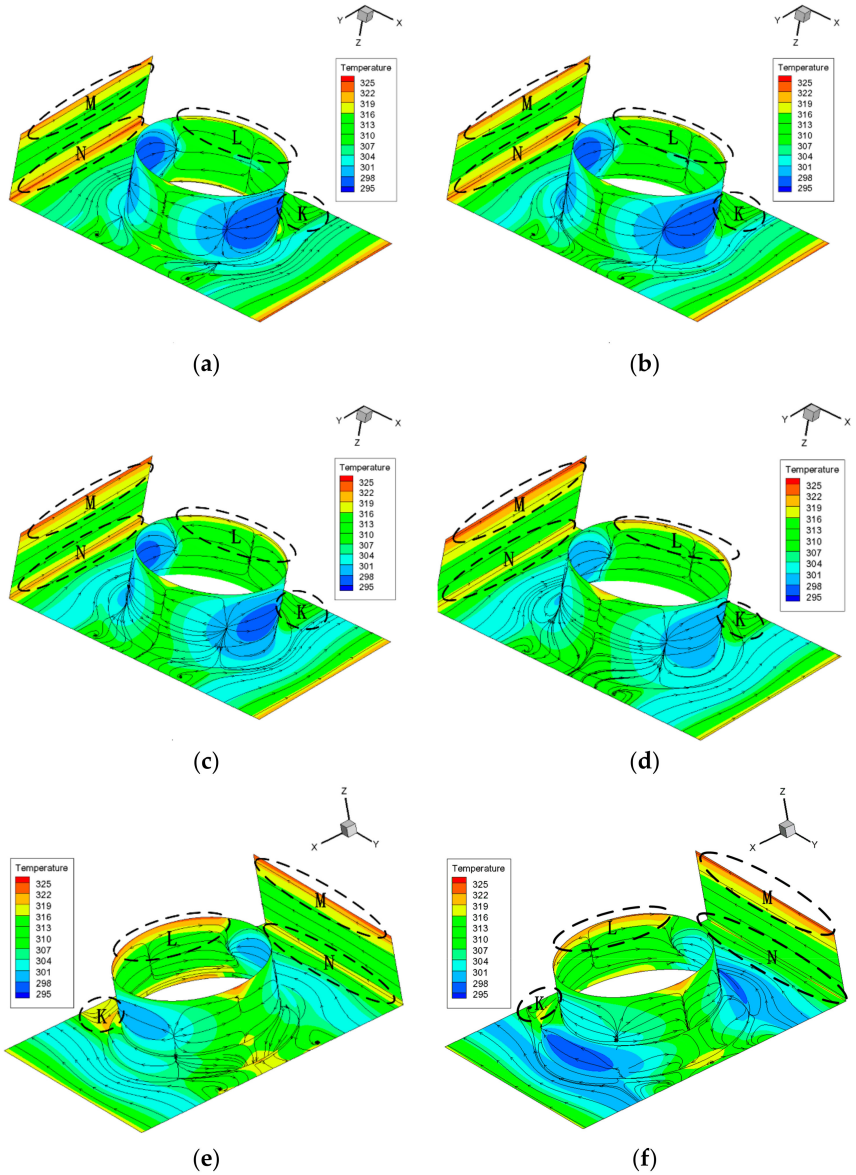

Figure 3. The distribution of temperature (unit: K) and limiting streamlines on the wall (*Re* = 200): (**a**) *r* = 0 μm; (**b**) *r* = 5 μm; (**c**) *r* = 10 μm; (**d**) *r* = 15 μm; (**e**) *ro* = 10 μm; (**f**) *ro* = 15 μm.

The distribution of temperature field and streamlines in the stream-wise mid-session surface with the radius of the fillet and bulb ranging from 2 μm to 15 μm are shown in Figure 4. Only half of the area is given because the structure is symmetrical.

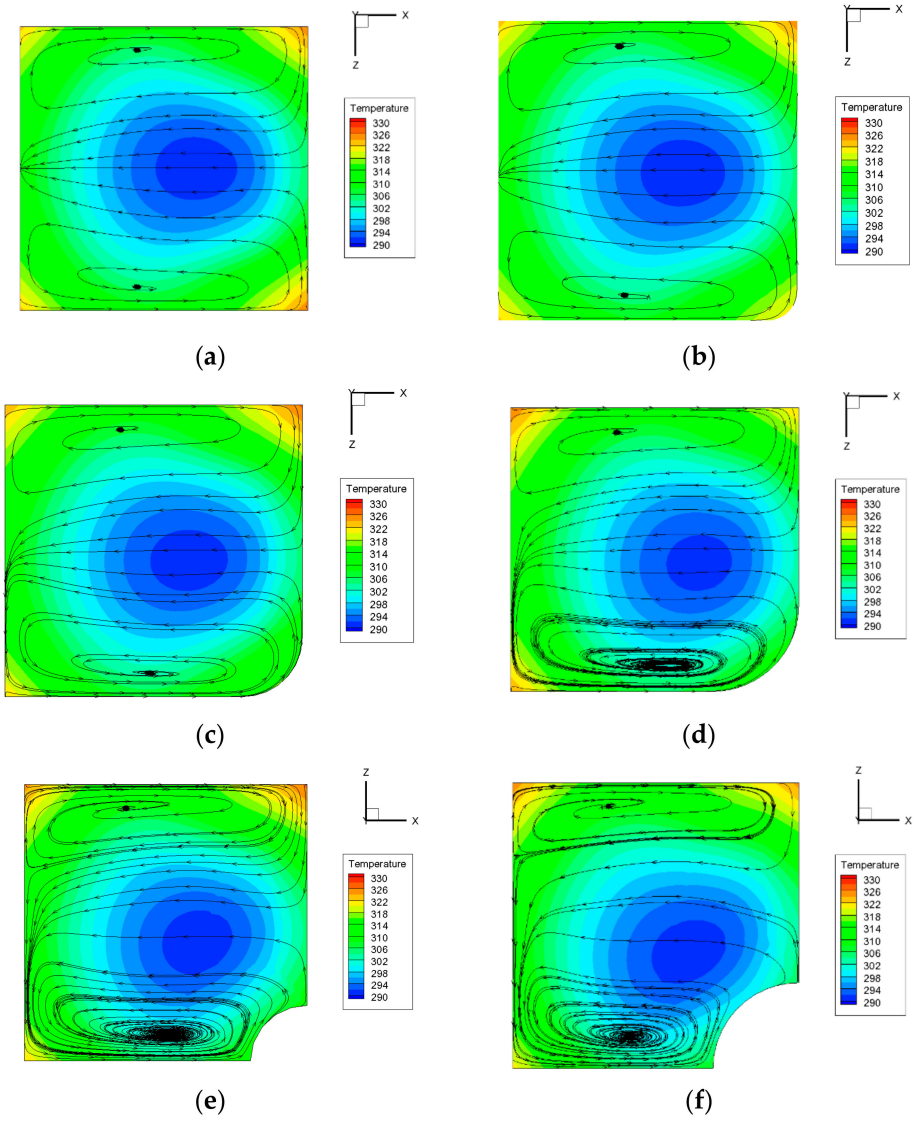

Figure 4. The distribution of temperature (unit: K) and streamlines in the stream-wise mid-session surface (*Re* = 50): (**a**) *r* = 0 μm; (**b**) *r* = 5 μm; (**c**) *r* = 10 μm; (**d**) *r* = 15 μm; (**e**) *ro* = 10 μm; (**f**) *ro* = 15 μm.

As shown in Figure 4, the channel is full of strong secondary flow. When *Re* is 50, in smooth microchannel, the secondary flow is symmetrical in the normal-wise direction. As for the case with a 15 μm fillet, due to the asymmetrical geometry structure, the secondary flow is no longer symmetrical, with a stronger secondary flow at the bottom and a weakened one at the top. It is worth noting that with the increment of the radius the secondary flow at the bottom expands upwards and gradually secondary flow in these two areas merges together into one. A similar trend is observed in the microchannel with bulbed pin-fin. The main low temperature region of those in smooth channel is symmetrical, circular and in the central of the channel while the region of those with fillet and bulb is asymmetrical and moves downwards, getting closer to the fillet and bulb. The maximum temperature is lower in those with fillet and bulb than that of smooth channel, especially in the regions near the fillet and bulb. The decrease of maximum temperature contributes to the decrease of the temperature gradient. It can be explained by the fact that after adding the fillet and bulb, the secondary flow,

developing from two separate ones into one, has enhanced the heat transfer near the vortex region and thus the uniformity of the temperature field is strengthened. We can also find that in the microchannel with bulb, the secondary flow in the bottom is more violent than that in the channel with the fillet while the interaction between two secondary flows in different regions is weaker than that in the channel with fillet. It can be explained by the fact that in the channel with bulbed pin-fin, two enormous changes in geometrical structure, one of which is in the edge of the bulb and the bottom wall and the other one is in the edge of the bulb and the pin-fin surface. The first geometrical change has contributed to enhance the secondary flow at the bottom while the latter one hinders the development of the secondary flow upwards and thus weakens the interaction between the two areas.

Figure 5 shows that when Re = 200, the span-wise secondary flow both at the bottom and top is confined to the corner, its intensity is relatively less than that in the case of Re = 50. The influences of fillet and bulb on the flow structure decreases, and the interaction of the upper and lower secondary flow is no longer obvious. However, the fillet and bulb have a great influence on the temperature distribution. As the radius increases, the mainstream low temperature core region is obvious asymmetry, and it moves downwards gradually. The lower secondary flow is more violent than that in the smooth structure, and thus enhances the heat transfer performance of the bottom wall. Besides, the increase of secondary flow constrains the high temperature area to the corner, reduces the average temperature and enhances the heat transfer performance. However, because of the movement of the mainstream low temperature core region, the temperature of the upper fluid rises, leading to the heat transfer deterioration of the top wall which is consistent with the result of Figure 3. All the effects mentioned above are strongest when radius is 15 μm.

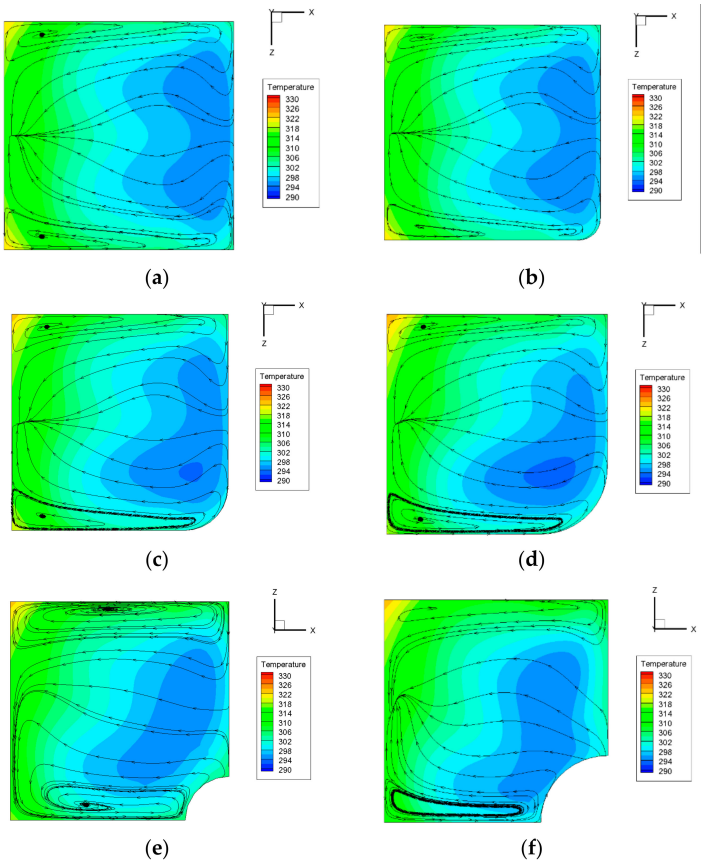

Figure 5. The distribution of temperature (unit: K) and streamlines in the stream-wise mid-session surface (Re = 200): (**a**) r = 0 μm; (**b**) r = 5 μm; (**c**) r = 10 μm; (**d**) r = 15 μm; (**e**) ro = 10 μm; (**f**) ro = 15 μm.

3.2. Performance Parameters Analysis

The fillet and bulb influence the flow pattern and the distribution of temperature field. From the above analysis, it is obvious that the fillet and bulb can lower the maximum wall temperature, improve thermal uniformity of the wall and enhance the heat transfer efficiency. However, the change of the cross-sectional area and the flow field will also influence the flow resistance. The flow drag, heat transfer performance parameter and the comprehensive heat transfer performance of the channel with the fillet and bulb are analyzed in the following.

3.2.1. Flow Resistance Analysis

The Fanning friction factor f, form drag C_p and frictional resistance C_f are compared in order to analyze the resistance of fluid. The definition of Fanning friction factor is given by Formula (9). The frictional resistance C_f, and form drag C_p are given by

$$C_f = \frac{X_w}{0.5\rho U_{ave}^2}, C_p = f - C_f \tag{16}$$

where X_w is the wall shear stress, C_p/f and C_f/f indicate the proportion of form loss and friction loss in the Fanning friction factor, respectively.

Figure 6 shows the influence of the fillet and bulb on f. As for the microchannel with filleted pin-fin, f is almost the same with the smooth pin-fin microchannel except for cases when r = 15 μm and r = 10 μm, Re = 50. When the radius of the fillet increases, the flow resistance increases slightly, the maximum increase percentage is only 2.03%. This is mainly due to the slight decrease of the flow passage regions as the radius of the fillet increases. The results show that the fillet structure will not notably increase the flow resistance. As for the microchannel with bulbed pin-fin, the radius influences f a lot. f/f_0 increases a lot as the radius increases and is much larger than the others when radius is greater than 10 μm. All these influences decrease as the Reynolds number increases. The maximum increment percentage is 13.48% when r = 15 μm, Re = 50. The bulb increases the flow resistance as the radius increases.

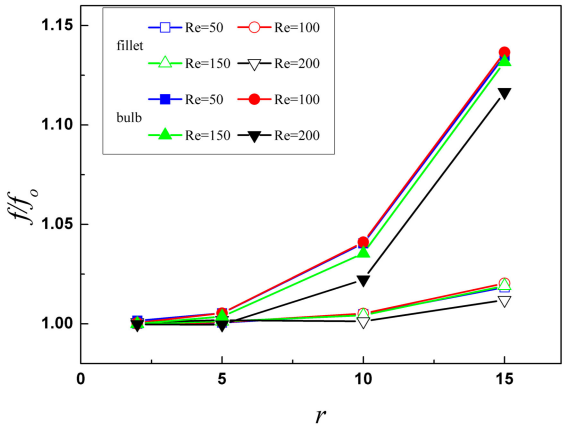

Figure 6. Variation of f/f_0 with radius.

Figure 7 is shown to explain how the fillet and bulb influence f. The Fanning friction factor consists of frictional resistance C_f and form drag C_p, so the increment of the f also consists of two parts. $(C_p - C_{p0})/f_0$ represents form drag increment and $(C_f - C_{f0})/f_0$ represents frictional resistance increment. Figure 7 shows that the fillet has little influence on C_p and C_f, so it well explains the influence of fillet on f. However, for the microchannel with bulbed pin-fin, both C_p and C_f increase, and C_p increases more significantly. When radius increases to 10 μm or 15 μm, the proposed structure advances and extends the reflux region, which induces the increase of C_p of the microchannel when it

has a relatively larger radius. The larger the radius is, the more the form drag generates. This is why $(C_p - C_{p0})/f_0$ is larger than the others.

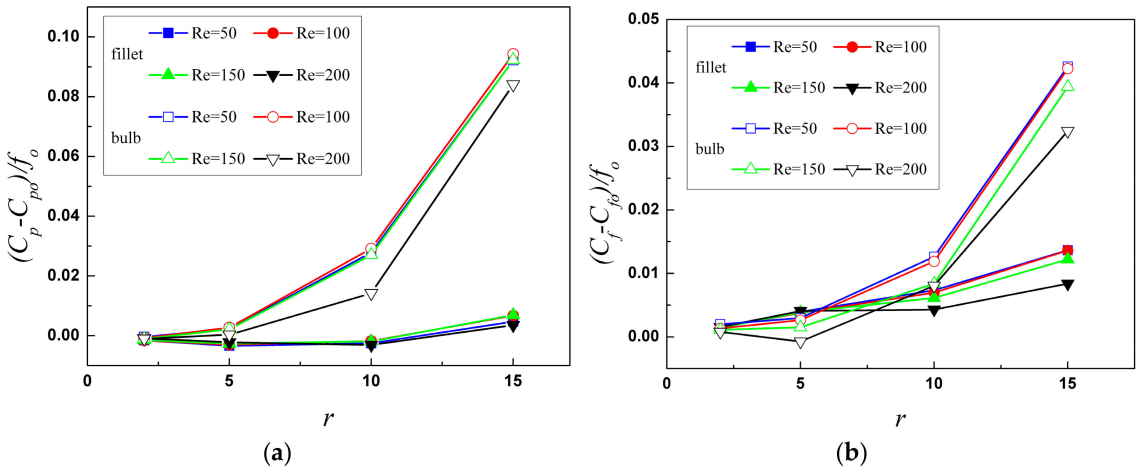

Figure 7. Friction increase of two compoents: (**a**) form drag C_p; (**b**) frictional resisitance C_f.

3.2.2. Heat Transfer Effect Analysis

The variations of *Nu* (defined by Equation (6)) at different cases are shown in Figure 8. For cases of microchannels with filleted pin-fin, *Nu* increases with the increase of radius at low *Re* and adverse tendency is observed at relatively high *Re*. It is because in low *Re* flow, heat transfer augmentation increases as the radius increases. However, the augment weakens with the increases of *Re* and disappears when *Re* reaches 120. Then, heat transfer begins to deteriorate and the extent of deterioration increases with the radius increasing. This is because that the highest temperature region has changed from the rear of the cylinder to vortex region near the corner when *Re* changes from 50 to 200. A similar tendency appears in the cases with bulbs except that, for microchannels with a 5 μm or 10 μm bulb, the increment disappears when *Re* is 90; for those with a 15 μm bulb, the augment disappears when *Re* is 160.

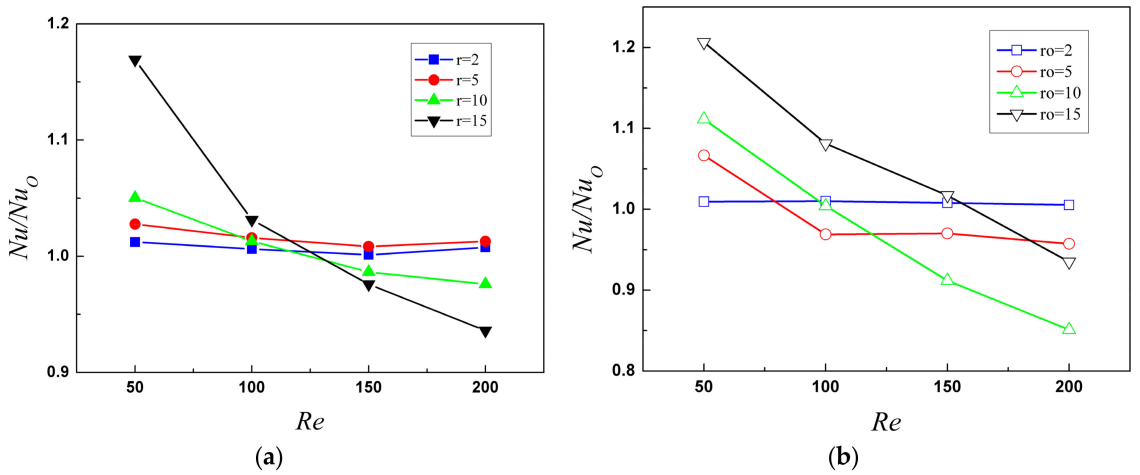

Figure 8. Variation of *Nu* with *Re*: (**a**) microchannel with filleted pin-fin; (**b**) microchannel with bulbed pin-fin.

3.2.3. Entropy Generation Analysis

Entropy generation indicates the fluid frictional irreversibility and heat transfer irreversibility in the forced conductive flow with heat transfer, and the relative entropy generation is used to evaluate flow loss and heat transfer performance in this work, based on the entropy generation theory and

Equation (15). As shown in Figure 9, the total relative entropy generation increases with the increment of *Re* in the microchannel with filleted pin-fin. The greatest increments, appearing when r = 15 μm, increase from 0.86 to 1.04 with the increase of *Re*. While in other cases, the increase is relatively smaller. It is worth noting that the increment magnitude increases with the radius increasing. It can be explained that, as it is revealed in Figures 4 and 5, secondary flow is enhanced with the increase of the fillet radius, which causes a higher loss, and with the increment of *Re*, secondary flows in those with larger fillets change greater. The increase rate of entropy generation decreases with the increase of *Re* in all cases. It is because secondary flows are depressed at high *Re*. Therefore, the loss has a tendency to decrease. However, the increase of *Re* will increase the flow loss and this effect surpasses the tendency of loss to decrease caused by the secondary flow condition. Finally, the flow loss increases at a rate which decreases with the increase of *Re*. Besides, adding fillet can improve the flow performance in low *Re*. This effect weakens with the increase of *Re*, disappears when *Re* is 120 and then the flow performance begins to deteriorate. As for the microchannel with bulbed pin-fin, the changing range of entropy with *Re* is larger compared to those with fillet structures, which reveals a greater loss, but the tendency of entropy generation is similar: The increase rate of entropy generation decreases with the increase of *Re* and the increment magnitude increases with the bulb radius increasing. Also, adding bulb can improve the flow performance in low *Re* and this effect disappears when *Re* is under 100 for those with a 2 μm, 5 μm or 10 μm bulb and for those with a 15 μm bulb, the effect disappears when *Re* is above 100.

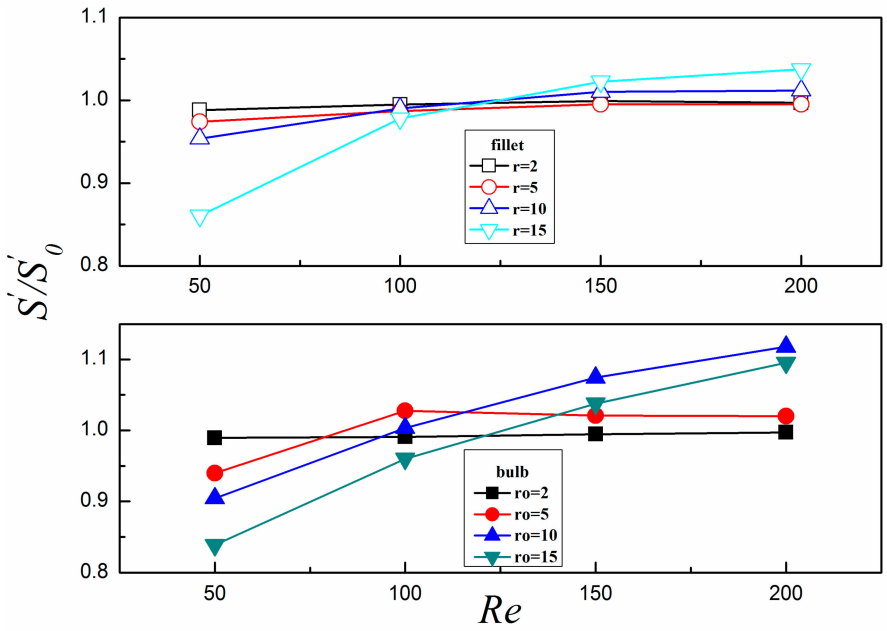

Figure 9. Variation of S/S'_0 in the microchannel with *Re*.

Heat transfer induced entropy generation is dominate for typical microchannel heat exchange systems [29]. As shown in Table 4, in low *Re*, heat transfer induced entropy generation reasonably constitutes the main part of the total entropy generation. Its proportion decreases with the increase of *Re*, which indicates an increasing frictional loss.

Table 4. Variations of S_T and S_F.

	S_T				S_F			
	50	**100**	**150**	**200**	**50**	**100**	**150**	**200**
r = 0 μm	0.969	0.835	0.633	0.453	0.031	0.165	0.367	0.547
r = 10 μm	0.967	0.832	0.635	0.459	0.033	0.168	0.365	0.541
ro = 10 μm	0.964	0.828	0.646	0.487	0.036	0.172	0.354	0.513

3.2.4. Synthetic Heat Transfer Analysis

The synthetic thermal performance TP takes both the heat transfer improvement and frictional loss penalty into account and it is frequently used to evaluate the heat transfer performance of devices. TP [30,31] is defined as

$$TP = \left(\frac{Nu}{Nu_0}\right) \cdot \left(\frac{f}{f_0}\right)^{-1/3} \tag{17}$$

where Nu_0 and f_0 refer to the relative data of channel with only a cylinder. The results are shown in Figure 10. ζ in Figure 10 is defined by

$$\zeta = \frac{TP_r - TP_0}{TP_0} \tag{18}$$

where TP_0 and TP_r refer to the data of benchmark without the fillet and bulb and data of those with fillet and bulb, respectively.

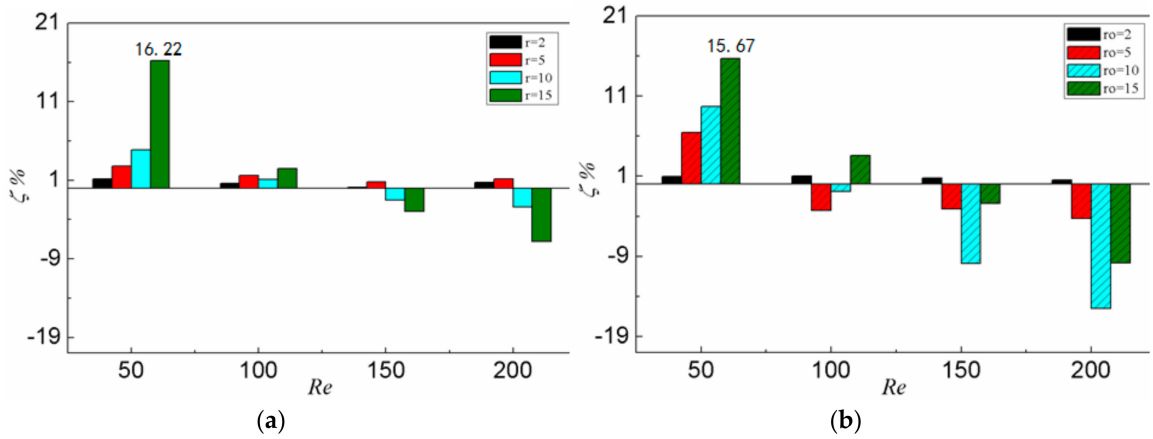

Figure 10. Variation of synthetic thermal performance with *Re*: (**a**) microchannel with filleted pin-fin; (**b**) microchannel with bulbed pin-fin.

As shown in Figure 10, obviously TP of both structures worsens with *Re* increasing. When *Re* is above 100, the thermal heat transfer augment of those with fillet or a 15 μm bulb disappears and then the heat transfer performance begins to deteriorate; for those with a 2 μm, 5 μm or 10 μm bulb, the thermal heat transfer augment disappears when *Re* is lower than 100, which is coherent with the entropy generation analysis. The extent of deterioration increases with the proposed structure becoming larger. For low *Re* flow, the highest temperature region is in the rear of the cylinder. Both fillet and bulb improve the heat transfer there and thus lead to thermal performance improvement. However, for high *Re* flow, the highest temperature region has changed from the rear of the cylinder to vortex region near the corner. Although the fillet and bulb still generate an improvement near the bottom area of the cylinder, heat exchange near the top area of the cylinder and vortex region in the corner begins to deteriorate, especially for those with bulb structures. The effect of the latter one surpasses the former one and thus causes deterioration of synthetic thermal performance. It is worth noting that

thermal performance of those with fillet structures performs better than those with bulb structures in relatively high *Re*, partly because of a greater augment in frictional loss in those with bulb structures.

4. Conclusions

The heat transfer performance and flow structures of laminar flow in the microchannels with endwall filleted pin-fin and bulbed pin-fin are investigated in this work. The conclusions obtained are as follows.

(1) Two separate symmetrical secondary flows develop in the microchannels with only a cylinder, with one on the top of the other. After adding the fillet and bulb, at low *Re*, the lower span-wise secondary flow is enhanced as the radius increases and these two span-wise secondary flows gradually merge into one which develops along the normal direction and improves the heat transfer performance in the channel. Both fillet and bulb strengthen the span-wise and the normal secondary flow in the channel, eliminate the high temperature area in the pin-fin, improve the heat transfer performance of the rear of the cylinder and enhance the thermal uniformity of the pin-fin and the outside wall. At high *Re*, the mainstream low-temperature core region is obvious asymmetry: It moves downwards gradually as *Re* increases.

(2) The flow resistance coefficient f of the microchannel with filleted pin-fin does not increase significantly compared to traditional microchannel with pin-fin, which means the use of the fillet can enhance the heat transfer while f of the microchannel is almost a constant. The maximum increase of f is 2.03%. As for the microchannel with bulbed pin-fin, f will not increase significantly when the radius is 2 μm or 5 μm, but when the radius increases to 10 μm or 15 μm, f increases a lot, and the maximum increase of f is 13.48%.

(3) For the microchannel with proposed structures, *Nu* increases as the radius increases in low *Re* flow and the adverse tendency appears in relatively high *Re* flow. *Nu* increases 16.93% at most for those with fillet and 20.65% at most for those with bulb. The increment of heat transfer performance decreases gradually as *Re* increases, and disappears when *Re* is 120 for those with fillet. As for microchannels with a 2 μm, 5 μm or 10 μm bulb, the increment decreases rapidly and disappears when *Re* is 90; for those with a 15 μm bulb, the augment disappears when *Re* is 160.

(4) Compared with the conventional pin-fin microchannel heat sink, the synthetic thermal performance coefficient *TP* of the new pin-fin microchannels increases by 16.22% at most for those with fillet and 15.67% at most for those with bulb.

Acknowledgments: The authors acknowledge the financial supports from the National Natural Science Foundation of China (Grant No. 61401227) and Natural Science Basic Research Plan in Shaanxi Province of China (Program No. 2017JQ5096).

Author Contributions: All authors have worked on this manuscript together, including the proposal of initial research concept and the design of research, as well as the data analysis and writing of manuscript, and all authors have read and approved the final manuscript.

Conflicts of Interest: The authors declare no conflict of interest.

Nomenclature

D_h	Characteristic length (μm)
F	Fanning friction factor
H	Microchannel height (μm)
h	Heat transfer coefficient ($W \cdot m^{-2} \cdot K^{-1}$)
Nu	Nusselt number
$q^{'}$	Heat transfer rate per unit length ($W \cdot m^{-1}$)
$q^{''}$	Surface heat flux rate ($W \cdot m^{-2}$)
r	Radius of fillet (μm)
ro	Radius of bulb (μm)
Re	Reynolds number
$S^{'}$	Entropy generation ($W \cdot m^{-1} \cdot K^{-1}$)
$S^{'}_F$	Friction induced entropy generation ($W \cdot m^{-1} \cdot K^{-1}$)
$S^{'}_T$	Heat transfer induced entropy generation ($W \cdot m^{-1} \cdot K^{-1}$)
T	Temperature (K)
TP	Thermal performance
U	velocity ($m \cdot s^{-1}$)
ΔP	Pressure drop (Pa)
ΔT	Mean temperature difference (K)

Greek Symbols

λ	Fluid thermal conductivity ($W \cdot m^{-1} \cdot K^{-1}$)
μ	dynamic viscosity ($Pa \cdot s$)
ρ	Fluid density ($kg \cdot m^{-3}$)

Subscripts

ave	Average
h	Hydraulic
w	Wall
o	Benchmark condition

References

1. Vafai, K.; Zhu, L. Analysis of two-layered micro-channel heat sink concept in electronic cooling. *Int. J. Heat Mass Transf.* **1999**, *42*, 2287–2297. [CrossRef]
2. Peles, Y.; Koşar, A.; Mishra, C.; Kuo, C.; Schneider, B. Forced convective heat transfer across a pin fin micro heat sink. *Int. J. Heat Mass Transf.* **2005**, *48*, 3615–3627. [CrossRef]
3. Fan, C.; Sun, F.; Yang, L.; Chen, L.; Qu, W.; Ma, T. Experimental investigation of flat miniature heat pipes with three kinds of micro grooves. *J. Enhanc. Heat Transf.* **2004**, *11*, 467–476. [CrossRef]
4. Xia, G.; Chai, L.; Wang, H.; Zhou, M.; Cui, Z. Optimum thermal design of microchannel heat sink with triangular reentrant cavities. *Appl. Therm. Eng.* **2011**, *31*, 1208–1219. [CrossRef]
5. Min, J.Y.; Jang, S.P.; Kim, S.J. Effect of tip clearance on the cooling performance of a microchannel heat sink. *Int. J. Heat Mass Transf.* **2004**, *47*, 1099–1103. [CrossRef]
6. Cheng, Y. Numerical simulation of stacked microchannel heat sink with mixing-enhanced passive structure. *Int. Commun. Heat Mass* **2007**, *34*, 295–303. [CrossRef]
7. Wei, X.; Joshi, Y.K.; Ligrani, P.M. Numerical simulation of laminar flow and heat transfer inside a microchannel with one dimpled surface. *J. Electron. Packag.* **2007**, *129*, 63–70. [CrossRef]
8. Li, P.; Xie, Y.; Zhang, D. Laminar flow and forced convective heat transfer of shear-thinning power-law fluids in dimpled and protruded microchannels. *Int. J. Heat Mass Transf.* **2016**, *99*, 372–382. [CrossRef]
9. Kosar, A.; Mishra, C.; Peles, Y. Laminar flow across a bank of low aspect ratio micro pin fins. *J. Fluids Eng. Trans. ASME* **2005**, *127*, 419–430. [CrossRef]

10. Kosar, A.; Peles, Y. Thermal-hydraulic performance of MEMS-based pin fin heat sink. *J. Heat Transf.* **2006**, *128*, 121–131. [CrossRef]
11. Marques, C.; Kelly, K.W. Fabrication and performance of a pin fin micro heat exchanger. *J. Heat Transf.* **2004**, *126*, 434–444. [CrossRef]
12. Vanapalli, S.; Ter Brake, H.J.M.; Jansen, H.V.; Burgrt, J.F.; Holland, H.J.; Veenstra, T.T.; Elwenspoek, M.C. Pressure drop of laminar gas flows in a microchannel containing various pillar matrices. *J. Micromech. Microeng.* **2007**, *17*, 1381–1386. [CrossRef]
13. Wang, Y.; Houshmand, F.; Elcock, D.; Peles, Y. Convective heat transfer and mixing enhancement in a microchannel with a pillar. *Int. J. Heat Mass Transf.* **2013**, *62*, 553–561. [CrossRef]
14. Chyu, M.K. Heat transfer and pressure drop for short pin-fin arrays with pin-endwall fillet. In Proceedings of the ASME 1989 International Gas Turbine and Aeroengine Congress and Exposition, American Society of Mechanical Engineers, Toronto, ON, Canada, 4–8 June 1989; p. V004T08A011.
15. Curlett, B.P. *The Aerodynamic Effect of Fillet Radius in a Low Speed Compressor Cascade*; NASA-TM-105347; NASA Lewis Research Center: Cleveland, OH, USA, 1991.
16. Hoeger, M.; Schmidt-Eisenlohr, U.; Gomez, S.; Sauer, H.; Müller, R. Numerical simulation of the influence of a fillet and a bulb on the secondary flow in a compressor cascade. *TASK Q.* **2002**, *6*, 25–37.
17. Hoeger, M.; Baier, R.D.; Müller, R.; Engber, M. Impact of a fillet on diffusing vane endwall flow structure. In Proceedings of the 11th International Symposium on Transport Phenomena and Dynamics of Rotating Machinery, Honolulu, HI, USA, 26 February–2 March 2006.
18. Kugeler, E.; Nürnberger, D.; Weber, A.; Engel, K. Influence of blade fillets on the performance of a 15 stage gas turbine compressor. In Proceedings of the ASME Turbo Expo 2008: Power for Land, Sea, and Air, Berlin, Germany, 9–13 June 2008; pp. 415–424.
19. Goodhand, M.N.; Miller, R.J. The impact of real geometries on three-dimensional separations in compressors. *J. Turbomach.* **2012**, *134*, 021007. [CrossRef]
20. Meyer, R.; Schulz, S.; Liesner, K.; Passrucker, H.; Wunderer, R. A parameter study on the influence of fillets on the compressor cascade performance. *J. Theor. Appl. Mech.* **2012**, *50*, 131–145.
21. Li, P.; Zhang, D.; Xie, Y. Heat transfer and flow analysis of Al_2O_3—Water nanofluids in microchannel with dimple and protrusion. *Int. J. Heat Mass Transf.* **2014**, *73*, 456–467. [CrossRef]
22. Mistry, K.H.; McGovern, R.K.; Thiel, G.P.; Summers, E.K.; Zubair, S.M.; Lienhard, V.J.H. Entropy generation analysis of desalination technologies. *Entropy* **2011**, *13*, 1829–1864. [CrossRef]
23. Li, P.; Xie, Y.; Zhang, D. Heat transfer enhancement and entropy generation of nanofluids laminar convection in microchannels with flow control devices. *Entropy* **2016**, *18*, 134. [CrossRef]
24. Shah, R.K.; London, A.L. *Laminar Flow Forced Convection in Ducts*; Academic Press: New York, NY, USA, 1978.
25. Yang, D.; Jin, Z.; Wang, Y.; Ding, G.; Wang, G. Heat removal capacity of laminar coolant flow in a micro channel heat sink with different pin fins. *Int. J. Heat Mass Transf.* **2017**, *113*, 366–372. [CrossRef]
26. Yang, D.; Wang, Y.; Ding, G.; Jin, Z.; Zhao, J.; Wang, G. Numerical and experimental analysis of cooling performance of single-phase array microchannel heat sinks with different pin-fin configurations. *Appl. Therm. Eng.* **2017**, *112*, 1547–1556. [CrossRef]
27. Zhao, J.; Huang, S.; Gong, L.; Huang, Z. Numerical study and optimizing on micro square pin-fin heat sink for electronic cooling. *Appl. Therm. Eng.* **2016**, *93*, 1347–1359. [CrossRef]
28. Hasan, M.I. Investigation of flow and heat transfer characteristics in micro pin fin heat sink with nanofluid. *Appl. Therm. Eng.* **2014**, *63*, 598–607. [CrossRef]
29. Li, J.; Kleinstreuer, C. Entropy generation analysis for nanofluid flow in microchannels. *J. Heat Transf.* **2010**, *132*, 122401. [CrossRef]
30. Xie, G.; Liu, J.; Zhang, W.; Lorenzini, G.; Biserni, C. Numerical prediction of flow structure and heat transfer in square channels with dimples combined with secondary halfsize dimples/protrusions. *Numer. Heat Transf. A Appl.* **2014**, *65*, 327–356. [CrossRef]
31. Murata, A.; Mochizuki, S. Centrifugal buoyancy effect on turbulent heat transfer in a rotating two-pass smooth square channel with sharp 180-deg turns. *Int. J. Heat Mass Transf.* **2004**, *47*, 3215–3231. [CrossRef]

© 2017 by the authors. Licensee MDPI, Basel, Switzerland. This article is an open access article distributed under the terms and conditions of the Creative Commons Attribution (CC BY) license (http://creativecommons.org/licenses/by/4.0/).